Ninth International Conference on
THIN-WALLED STRUCTURES – ICTWS2023
Sydney, Australia, Nov 29 – Dec 1, 2023

EXPERIMENTAL AND NUMERICAL STUDY ON SLENDER CONCRETE-FILLED STEEL TUBULAR ARCHES SUBJECTED TO TILTING LOADS

Yue Geng*, Jiaqi Sun*, Hao Zhang, Haitang Yin* and Yuyin Wang***

* Harbin Institute of Technology
e-mails: gengyue@hit.edu.cn, sunjiaqi@stu.hit.edu.cn, yinhaitang2012@163.com, wangyuyin@hit.edu.cn

** The University of Sydney
e-mail: hao.zhang@sydney.edu.au

Keywords: Concrete filled steel tube, Arch, Tilting load, Confinement effect, Buckling behaviour.

Abstract. *The CFST arches usually have a large slenderness ratio, which makes the arches more prone to buckling. Despite this, limited experimental investigations have been performed on the buckling behaviour of CFST arches. In this study, a buckling test was performed on one 9 m long CFST parabolic fixed arches with single circular cross-section subjected to central concentrated tilting load. A loading rig was designed for performing the buckling test on the slender CFST arches subjected to the 'tilting load'. The loading rig ensured that the applied tilting load always passed through the centroid of the cross section, allowing the arch to deform freely in the out-of-plane direction, except for the restraint of the suspenders and preventing unexpected unloading induced by the sudden increase in the deflection at the buckling point. Based on the test results, FE models using solid elements and a simplified beam FE model were built to investigate the confinement effects on buckling behavior of the tested CFST arch. Relatively significant confinement effects were found on the arches and were considered in the FE modelling. Both the built FE models using solid and beam elements performed well in predicting the buckling behaviour of the CFST arches.*

1 INTRODUCTION

The use of concrete-filled steel tubular (CFST) arches is becoming popular for bridge applications. Till 2023, more than 600 CFST arch bridges have been built in China. With the improvements in material and construction techniques, the span of newly built CFST arch bridges continues to increase, and the longest span has reached 575 m. Long-span arch bridges are more prone to out-of-plane buckling, and thus, if the bridge deck hangs using flexible suspenders and with a high out-of-plane stiffness, the suspenders incline and generate tilting loads. The tilting loads restrain the further out-of-plane deformation of the arch rib and increase its load-carrying capacity significantly.

Despite of the increasing use of CFST arches, limited experimental research has been conducted on the buckling behavior of the arches. For the in-plane stability, Liu et al. [1] experimentally highlighted the significant influence of the rise-to-span ratios. Huang et al. [2] tested four additional parabolic CFST arches to investigate the influence of the initial stress levels in hollow steel tubes. Fewer experiments have been carried out on the out-of-plane buckling behavior of arches. The tested specimens included a parabolic arch with a circular cross section [3] and seven parabolic twin-arches [4]. Among the eight tested specimens, only one specimen in reference [3] was subjected to tilting loads, for which the measured load-displacement curve had no descending branch. To date, no CFST arch has been tested to failure under a central concentrated tilting load, which is also representative loading cases in real CFST

arch bridges. It is unclear and controversial whether the confinement effects should be considered in the modelling of slender CFST arches.

To provide benchmark data for finite element models, this study performed experimental investigation on one 9 m long CFST parabolic fixed arch with single circular cross-section subjected to central concentrated tilting load. A loading rig was designed with the capability of 1) obtaining the descending branches of the load-displacement curves, 2) applying the tilting load without introducing additional restraining force, and 3) allowing free lateral deformations of the arch, except for the restraint of the suspenders. Based on the test results, FE models using solid elements and a simplified beam FE model were built to investigate the confinement effects on buckling behavior of the tested CFST arch.

2 EXPERIMENTAL PROGRAMME

2.1 Loading cases and parameters of the tested arch

Figure 1 presents the loading cases of the 9 m long CFST parabolic arch under central concentrated load (named as Arch-1/2). The arch was fixed at the ends. Flexible suspenders were adopted to apply the concentrated vertical loads, with bottom ends restrained in the out-of-plane direction at the height of the arch springing, while allowed to deform freely in the vertical direction.

The arch is slender with the in-plane slenderness ratio of λ_x=92.5 and out-of-plane slenderness ratio of λ_y=190.3. Meanwhile, the tested arch has a low steel ratio α=7.5%. The outer diameter and the thickness of the hollow steel tube is D=140 mm and t=2.5 mm, respectively. The arch axis follows the Eq. (1):

$$y = -\frac{x^2}{9000} + 2250 \quad (-4500\text{mm} \le x \le 4500\text{mm}) \tag{1}$$

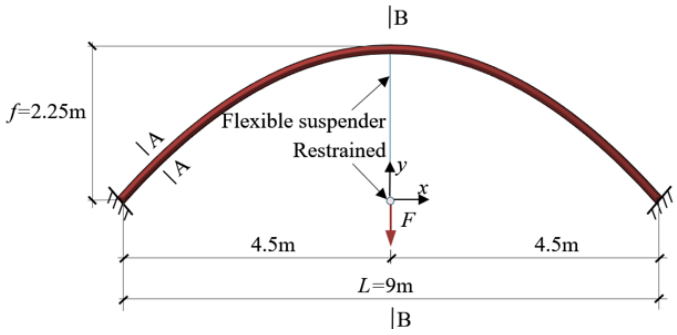

Figure 1. Loading cases of the tested arch.

2.2 Material properties

The measured results for the mechanical properties of the steel tubes include: the elastic modulus E_s=2.09×105 MPa; yield strength f_y=330 MPa; ultimate tensile strength f_u=430 MPa and proportional limit f_p=0.7f_y=231 MPa. The Poisson's ratio for the steel tube μ_s is 0.275. The mean 28 day compressive strength $f_{cu,28}$=47.6 MPa. The equivalent concrete cylinder strength at the test date was f_{cm}=51.5 MPa. The elastic modulus at the test date was E_c=3.08×10^4 MPa and the Poisson's ratio was μ_c=0.19.

2.3 Preparation of specimens

The hollow steel arches (with the arch axis length of 10.33 m) were made of 3 segments, which were welded together with complete joint penetration (CJP) weld. The locations for the two connecting points were carefully selected to minimize its influence on the arch performance. The hollow steel arches were hot-bent with the dried fine sands fully filled inside the steel tube to prevent the local buckling. Then the concrete was poured from both ends of the tubes with the steel tubes placed upside down and was well compacted. A hole with a diameter of 40 mm was cut on the bottom surface of the arch crown to avoid air-induced void during the concrete pouring and was restrengthened by a cover steel plate after the hardening of the concrete core. To avoid end failure of the arch, stiffeners were welded to the arch springings.

Particular attention was paid to make sure that the concrete and steel tube can work together during the loading process. Specifically, the core concrete was initially poured with the elevation higher than that of the outer steel tube at both ends of the arches. One month after concrete pouring, the top surfaces of the concrete were ground into the same plane of the outer steel tube to make sure that the loads were exerted on the whole composite cross-section. To minimize the shrinkage effect, the exposure time of the concrete core was strictly controlled by tightly wrapping aluminum sheets around the top surfaces of the specimens and the holes on the arch crowns right after the concrete pouring. The concrete grounding and the steel end plate welding were conducted immediately after removing the aluminum sheets. With the above measures, the concrete and the steel could be considered as fully bonded due to the small autogenous shrinkage of core concrete (only 13με according to the Eurocode 2 model).

2.4 Loading rig

For slender arch with long span length, one crucial issue is that significant displacement increase in very short time may occur at the arch buckling. To ensure the stableness of the load, the springs with low stiffness were adopted in the loading rig (Figure 2a) to compensate the fast deflection increase.

The loads were applied through hydraulic jacks placed beneath the springs and were monitored by the load cells placed beneath the reaction beam (Figure 2a). Four threaded steel rods were fastened against the top and bottom steel plates with nuts, which passed through the reaction beam, springs and two middle steel plates freely. Particular attention was paid to ensure that all the above devices (including the steel plates, the load cell, the springs, the hydraulic jack and the steel rods) were geometrically center aligned.

A lateral resistance device (Figure 2b) was adopted to simulate the lateral restraint of the bridge deck to the out-of-plane deflection of the arch. All the milled lateral resistance plates were remained strictly vertical by adjusting the bolts on the reaction frame. Rollers were adopted to allow the arch to deform freely in the vertical direction while restrained in the lateral direction at the arch springing elevation. To ensure that all the rollers were placed right against the lateral resistance plates, the lengths of the horizontal steel rods were adjustable using threaded sleeves. The flexible suspenders passed through the hole in the lifting handle of the loading rig and fixed with U-shaped clips. The locations of the loading rigs were carefully adjusted to ensure that all the holes of the lifting handle (at the same level as the rollers) were in the line that connecting the two arch springings.

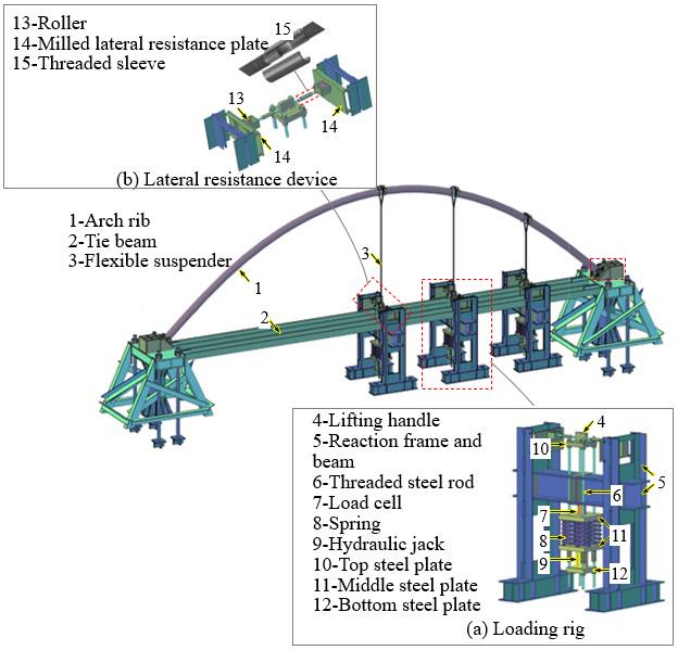

Figure 2. Test set-up for the buckling test on CFST arch.

2.5 Loading process

At the initial loading stage, the load interval was 5 kN for Arch-1/2 and 2 kN for Arch-3-points. At each load interval, the loads were sustained for 1 min to obtain the steady data. In this stage, the loading rate was 0.8 kN/min for Arch-1/2 and 0.2 kN/min for Arch-3-points. After reaching 70% of the predicted peak load, the test was transformed into displacement control, with the rate of 40 mm/min for the specimen Arch-1/2 and 18 mm/min for the specimen Arch-3-points at the middle suspender. For the specimen Arch-1/2, the test was terminated when the load reduced to $0.9F_u$ (where F_u represents the peak load of the applied load). For the specimen Arch-3-points, the test was terminated when the loads reduced to 0.98 F_u as the in-plane displacements of the arches were too large.

Particular method was adopted to ensure that the loads at different locations of the specimen Arch-3-points could be applied synchronously with the same value and the maximum difference was 3% during the whole loading process.

2.6 Displacement and strain measurements

Three displacement measuring systems were adopted in this test, including the LVDTs, the stereo vision system, and the total station measuring system. The LVDTs were placed in the *y* and *z* directions at 5 points with equal intervals along the arch span length (Figure 3) to measure the in-plane and out-of-plane displacements of the arches. At each arch springing, the LVDTs were placed in the *x* and *z* directions (Figure 3) to measure the two horizontal displacements.

Unlike the in-plane buckling tests in which the LVDTs and the specimens were always remain in the same plane, in this test, the LVDTs would change their location relative to the arch specimen due to the out-of-plane deformation of the specimens. To prevent this influence, a relatively large glass slide (with the dimension of 200 mm×200 mm, see Figure 3) was adopted for the LVDT to point to. This glass slide was greased to further reduce the friction as the LVDT slipped aside from the arch specimen during the experiment. To ensure that the glass slide was in perfect vertical or horizontal plane, a pedestal base consisting of three adjustable legs was adopted to place and fix the glass slide.

Stereo vision system was also adopted to measure the *x*, *y* and *z* deflections of the arches during the whole loading process. For this measuring system, circular targets were attached at the same positions as the LVDTs (Figure 3). The diameter of the circular target was 400 mm and the width of the outer black ring was 100 mm. In this test, the stereo vision measuring system (which is consisted of two CCD cameras) was kept 8 m away from the arch specimen, 4.5 m away from the ground. The two Pike-F-100c CCD cameras could record images with a pixel resolution of 1,000×1,000 at 10 fps automatically and the cameras were equipped with the optical lenses with 5 mm focal length. Detailed noncontact measurement method can be referred to.

The total station has an angle measurement accuracy of 2″ and a distance measurement accuracy of 1.5 mm ± 2.0 ppm. The distance between the total station and the arch specimen was 3 m. In this context, the measuring error of the total station was 0.0011 mm. During the test, the reflective targets were attached at the center of the circular targets (Figure 3). Due to the time required for the data reading for total station system, this measurement system was only adopted to measure the *x*, *y* and *z* deflections of the specimens in the step loading stage.

It is worth mentioning that the effect of the torsional twist of the cross-section was not measured in this investigation because the torsional rigidity of the circular cross-section was large and the out-of-plane displacements of the arches was small, which barely influence the buckling behavior of the tested arches.

The strains of the steel tubes were monitored using strain rosettes at representative cross-sections, i.e. at the arch crown, the quarter points and the arch springings (Figure 3). At each cross-section, four strain rosettes were attached to the upper, bottom, front and rear edge of the arch rib, respectively (Figure 3). The strains at the arch crown were measured by two groups of strain rosettes that symmetrical to the arch crown with the horizontal distance of 150 mm (Figure 3).

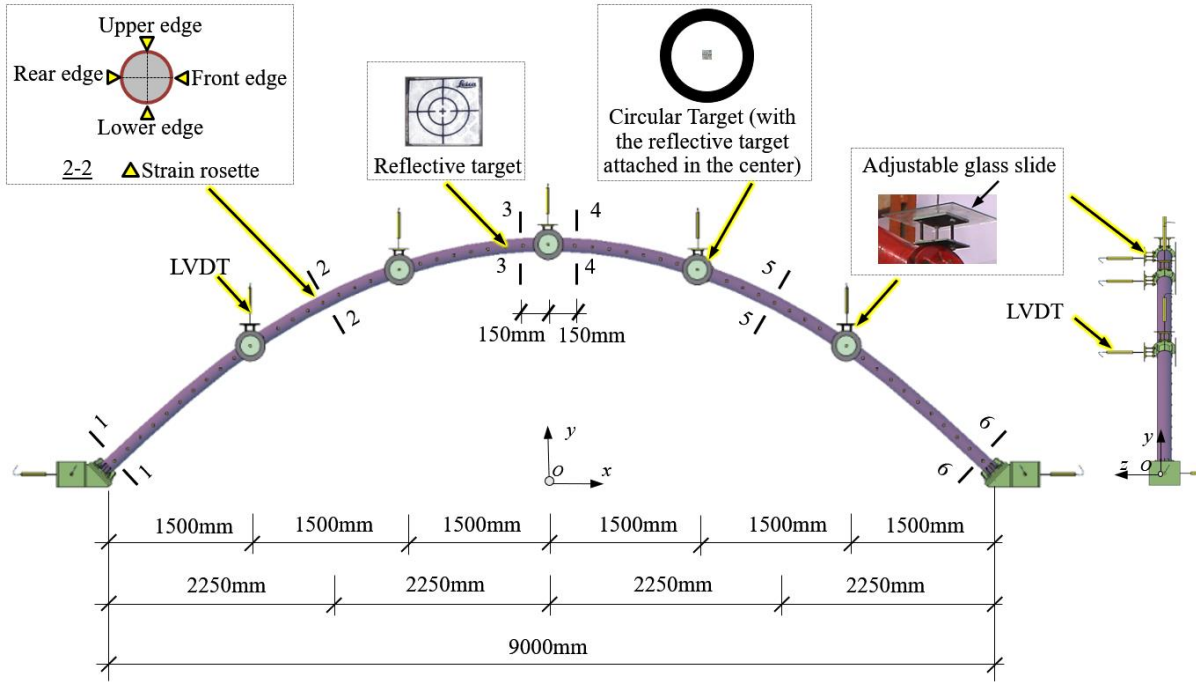

Figure 3. Instrumentation layout for the buckling test on CFST arches.

3 EXPERIMENTAL RESULTS

3.1 Load-displacement curves

As expected, the displacements in the *y* and *z* directions are initially increased linearly with the applied loads (Figure 4). After reaching approximately 60% of the peak load, the displacements increase at a higher rate. After reaching the peak load, the load-displacement curves of both tested specimens begin to descend with the displacements increasing rapidly.

The in-plane deflections are more pronounced than those in the out-of-plane direction. Arch-1/2 has the maximum out-of-plane displacement of 6 mm, which is only 5% of the in-plane one.

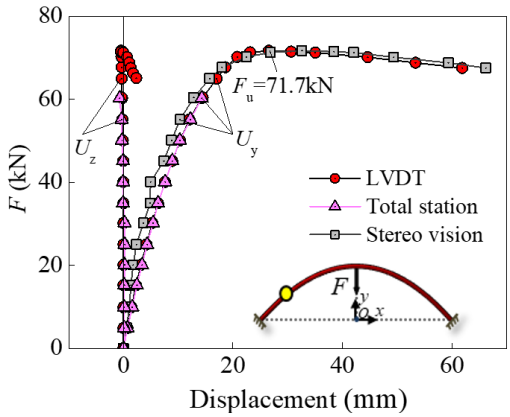

Figure 4. Typical load-displacement curves of the specimen Arch-1/2 (U_y, U_z).

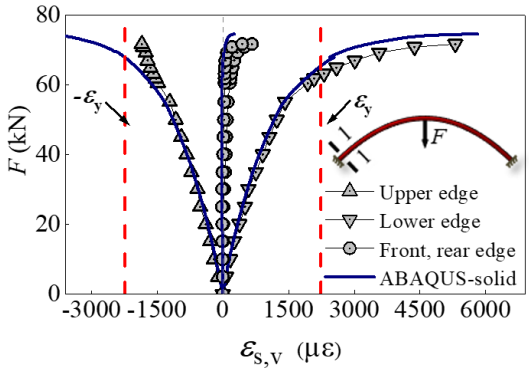

Figure 5. Comparison of the experimental and predicted typical load-strain curves of the specimen Arch-1/2.

3.2 Load-axial strain curves

Figure 5 present the typical axial strain ($\varepsilon_{s,v}$) versus load (F) curves for the specimen Arch-1/2, respectively. The results predicted by the FE models using solid elements are also presented in Figure 5, which will be discussed in Section 4.1. In Figure 5, negative value represents compressive strain. As expected, the strains at the upper and bottom edges are much higher than those at the front and rear edges. The cross sections have one measuring point under compression while the other three measuring points in tension and the compression sides are at the upper or bottom edge of the cross-sections. These measurement results are consistent with the observations from the load-displacement curves that the arch is mainly under in-plane deformation. These measured results also indicate that the arch is mainly under in-plane bending moment, while the axial compressions are relatively low.

4 FINITE ELEMENT ANALYSIS USING SOLID ELEMENTS

ABAQUS was adopted herein to establish the finite element model on fixed CFST parabolic arch. The concrete core, the outer steel tube and the flexible suspenders were modelled with C3D8R, S4R and T3D2, respectively.

The constitutive model of the steel tube was described by the uniaxial stress-strain curve obtained from the coupon test. The concrete damage plasticity model was employed to simulate the plastic behavior of the concrete with the key parameters following Tao's suggestion [5].

The arc-length method was adopted for the buckling analysis.

4.1 Model verification

Figure 6 compare the predicted and measured load-displacement curves. It can be noted that the FE results are close to the test ones. The results predicted by the models using beam elements are also presented, which will be discussed in Sections 5.2. and 5.3.

The load-axial strain curves obtained from the FE model are also very close to the measured ones (Figure 5).

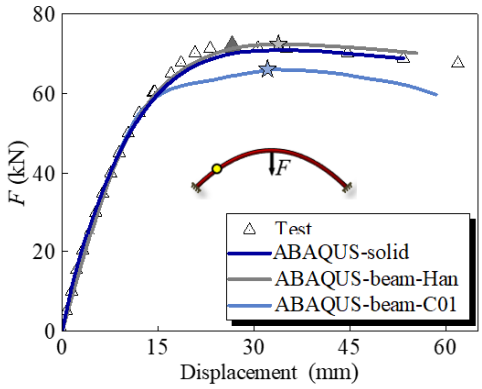

Figure 6. Comparison of the typical experimental and predicted load-displacement curves.

4.2 Confining pressure

The simulated results in Figure 7 can better present the confining pressure distribution in the tested CFST arch. It can be seen that the confining pressure distribute non-uniformly around the cross sections of the arch and basically all the cross-sections have the steel tubes circumferentially under tension with relatively large stress value, i.e., confining pressure exists. The maximum simulated circumferential stress of the steel tubes is 104.2 MPa.

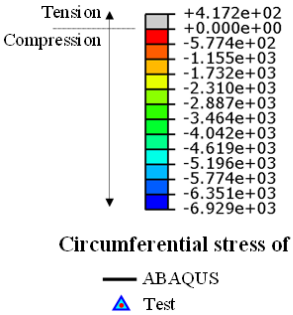

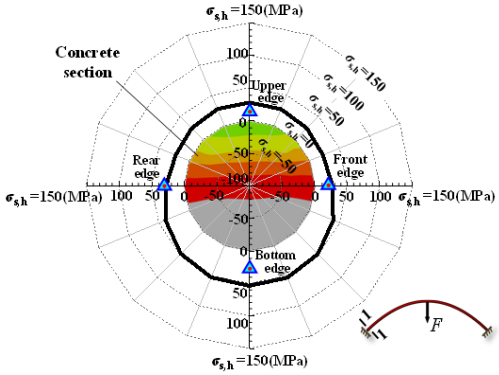

(a) Cross section 1-1

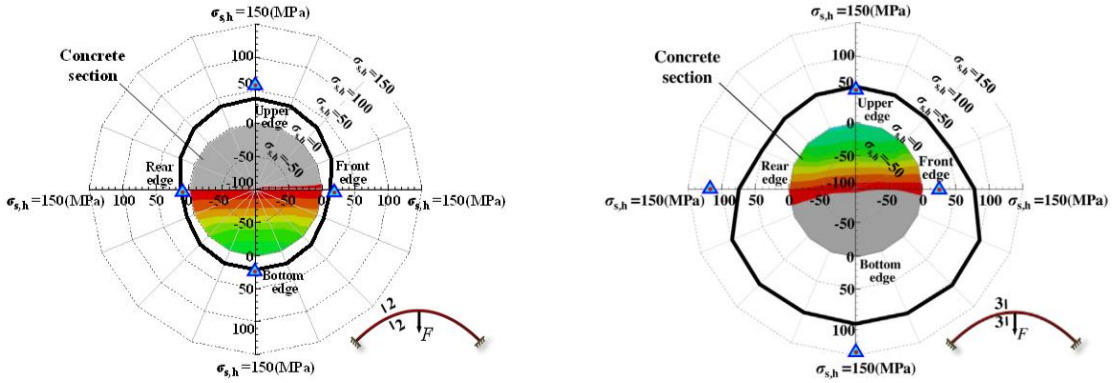

(b) Cross section 2-2 (c) Cross section 3-3

Figure 7. Measured and simulated circumferential stress distributions of the steel tube ($\sigma_{c,v}$) and axial stress nephograms of the concrete core ($\sigma_{s,h}$).

5 FINITE ELEMENT MODELLING USING BEAM ELEMENTS

The concrete core and the steel tubes were modelled using Timoshenko beam elements B31. The flexible suspenders were simulated by truss element T3D2.

5.1 Material properties

The measured stress-strain relationship of the steel tube was adopted for the modelling. Confining pressure was observed in a large portion of the tested arch as has been discussed in Section 4.2. To investigate whether the confinement effects need to be accounted in the FE modelling, both the confined concrete model provided by Han [6] and the unconfined concrete model of Concrete 01 [7] were adopted in the FE modelling for comparison purpose.

5.2 Model verification

Figure 6 compare the load-displacement curves of the specimens and the simulated results with the two concrete models. It can be noted that the simulated results with Han model are very close to the test results. The difference between the simulated and measured ultimate load-carrying capacity is only 0.9%.

5.3 Influence of the confinement effects

Compared with the simulated results with Han model, those with C01 model have much larger differences from the test results. In particular, the simulated peak load is 7.9% lower than the tested one (Figure 6). This highlights the necessity of considering the confinement effects in the FE modelling.

6 CONCLUSIONS

A loading rig was designed for performing the buckling test on the slender CFST arches subjected to the ‘tilting loads’. One 9 m long CFST parabolic fixed slender arches subjected to central concentrated load with a single circular cross-section was tested for failure. Three displacement measuring systems, including an LVDT system, stereo vision system, and total station measuring system, were adopted. FE models using solid elements and beam elements were built and validated against the test results. Using the FE model and test results, the confinement effects on the buckling behavior of the composite arches were evaluated. The main conclusions are as follows:

1) A relatively large confining pressure existed in the arch, and there were significant confinement effects on the ultimate capacity of the arch subjected to the central concentrated load and on the ductility of the arch subjected to the half-span three-point loads, which must be considered in the analysis.

2) The FE models built using solid elements and beam elements performed well in predicting the buckling behavior of the slender CFST arch.

REFERENCES

[1] Liu, C.Y., Wang, Y.Y., Wu, X.R. and Zhang, S.M. "In-plane stability of fixed concrete-filled steel tubular parabolic arches under combined bending and compression", *Journal of Bridge Engineering*, **22**(2), 04016116, 2017.

[2] Huang, F.Y., Cui, Y.L., Dong, R., Wei, J.G. and Chen, B.C. "Evaluation on ultimate load-carrying capacity of concrete-filled steel tubular arch structure with preload", *Advances in Structural Engineering*, **22**(13), 2755-2770, 2019.

[3] Chen, B.C., Wei, J.G. and Lin, J,Y. "Experimental study on concrete filled steel tubular (single tube) arch with one rib under spatial loads", *Engineering Mechanics*, **23**(5), 99-106, 2006 (in Chinese).

[4] Huang, Y.H., Liu, A.R., Zhu, C.J., Lu and H.W. "Experimental and numerical investigations on out-of-plane ultimate resistance of parallel twin-arch under uniform radial load", *Thin-Walled Structures*, **135**, 147-159, 2019.

[5] Tao, Z., Wang, Z.B. and Yu, Q. "Finite element modelling of concrete-filled steel stub columns under axial compression", *Journal of Constructional Steel Research*, **89**, 121-131, 2013.

[6] Li, W. and Han, L.H. "Seismic performance of CFST column to steel beam joint with RC slab: Joint model", *Journal of Constructional Steel Research*, **73**, 66-79, 2012.

[7] Kent, D.C. "Inelastic Behavior of reinforced concrete members with cyclic loading", *Bulletin of the New Zealand Society for Earthquake Engineering*, **4**(1), 108-125, 1971.